https://doi.org/10.1007/s41230-023-2122-6

Effect of sintering temperature on microstructure and properties of 3D printing polysilazane reinforced Al_2O_3 core

Wen-jun Dong[1], **Qiao-lei Li[2, 3], Tian-ci Chen[4], Ming-ke Zou[2], Jing-jing Liang[2, 5], Li-rong Liu[1], Hui Mei[6], and *Jin-guo Li[1, 2, 5]

1. School of Materials Science and Engineering, Shenyang University of Technology, Shenyang 110870, China
2. Shi-changxu Innovation Center for Advanced Materials, Institute of Metal Research, Chinese Academy of Sciences, Shenyang 110016, China
3. School of Materials Science and Engineering, University of Science and Technology of China, Shenyang 110016, China
4. School of Materials Science and Engineering, Northeastern University, Shenyang 110819, China
5. Space Manufacturing Technology (CAS Key Lab), Beijing 100094, China
6. Science and Technology on Thermostructural Composite Materials Laboratory, School of Materials Science and Engineering, Northwestern Polytechnical University, Xi'an 710072, China

Abstract: Ceramic cores are the key intermediate components of hollow blades for aero-engine. Conventional processes, such as hot-press molding and gel film casting, face difficulties in fabricating complex-structured ceramic cores due to the complexity of moulds and long process cycles. Stereolithography 3D printing provides a new idea for the fabrication of complex-structured ceramic cores. The effect of sintering temperature on open porosity, bulk density, weight loss rate, shrinkage rate, flexural strength and microstructure of the Al_2O_3-based ceramic core doped with 10vol.% polysilazane (PSZ) was studied. The sintering mechanism of PSZ-reinforced ceramic cores was analyzed. Results show that the optimum sintering temperature of PSZ-reinforced ceramic cores is 1,450 °C. At this temperature, the open porosity of the ceramic core is 36.60%, bulk density is 2.33 g·cm^{-3}, weight loss rate is 22.11%, shrinkage rate along the *X*, *Y*, *Z* directions is 5.72%, 5.01%, 9.61%, respectively; the flexural strength is 28.794 MPa at 25 °C and 13.649 MPa at 1,500 °C. Properties of 3D printing PSZ-reinforced ceramic cores can meet the casting requirement of superalloy hollow blades, which is expected to promote the industrial application of 3D printing complex structure ceramic cores.

Keywords: investment casting; ceramic core; 3D printing; sintering temperature; flexural strength

CLC numbers: TG221$^+$.1 **Document code:** A **Article ID:** 1672-6421(2023)05-387-08

1 Introduction

Ceramic cores are the key intermediate components of hollow blades for aero-engine, which affect the reliability and heat resistance of blades with complex cooling channels [1-5]. Therefore, the high precision of ceramic cores has been the goal of industry and academy. Conventional processes, such as hot-press moulding and gel film casting, are mature and high efficiency for ceramic cores with simple structures [6-8]. However, due to complexity of moulds and long process cycles [9, 10], these conventional processes cannot meet the requirements for the preparation of ceramic cores with high customization and complexity [11, 12]. Hence, a rapid and efficient preparation process for complex ceramic cores is needed.

Stereolithography 3D printing is a typical additive manufacturing (AM) process that is applicable to a wide range of materials. This process is characterized by short production cycle, low cost and high design freedom [13, 14]. Many researchers have fabricated ceramic cores with a slurry mixed by resin (liquid) and ceramic powders (solid) via stereolithography 3D printing. However, a new problem was found that the as-built cores are prone to cracking, deformation, and low strength. The defects of ceramic core can be improved to some extent by increasing the solid content of ceramic slurry [13]. At present, the solid content is

***Jin-guo Li**
Male, Ph. D., Researcher. His research interests mainly focus on superalloy precision casting, especially the ceramic mould casting.
E-mail: jgli@imr.ac.cn
****Qiao-lei Li**
E-mail: lql_614@163.com
Received: 2022-09-22; Accepted: 2023-03-22

typically above 50vol.% to ensure the strength of ceramic cores, and samples cannot be prepared when the solid content is below 40vol.% [2]. However, the printability will decrease when the solid content is above 55vol.% due to the increase of viscosity [15, 16].

In general, ceramic cores are required to meet the following requirements: (a) Open porosity is higher than 30%. If the open porosity is below 30%, there will be not enough space for corrosive liquid to corrode the ceramic cores. However, if the open porosity is too high, the strength of the ceramic cores will be decreased, causing cracks in the casting process. (b) Flexural strength at 25 °C is between 20–30 MPa and about 15 MPa at 1,500 °C [14]. Thus, to simultaneously meet these requirements, a balance between high ceramic-powder content and high printability needs to be found.

In recent years, ceramic precursors have been added to ceramic slurries to achieve increased ceramic content of cores after sintering while with little impact on the printability of stereolithography 3D printing [16, 17]. Through the addition of precursors into ceramics, the thermomechanical properties of ceramics can be improved without adding sintering additives [17]. He et al. [17, 18] added SiO_2 powders to epoxy acrylate siloxane to increase the ceramic content of photocured polysiloxane (PSO) precursor to solve the contradiction between high solid content and printing difficulty. During the sintering process, the PSO/SiO_2 precursor was converted into ceramic cores. The prepared ceramic cores have no cracks or pores, and exhibit good mechanical properties. Common ceramic precursors mainly include polysiloxane, polysilazane (PSZ), and polysiloxane containing silicon atoms in the main chain [19, 20]. After the green body is formed, precursors are converted into SiOC, SiCN and SiC ceramics by high temperature pyrolysis. Among them, PSZ has the advantages of low viscosity, short curing time, high ceramic content and good adhesion to ceramic materials. Therefore, doping PSZ into the ceramic slurry is an effective way to prepare cores of high ceramic content using a low solid content slurry.

In this study, PSZ was doped into the slurry for preparation of the Al_2O_3-based ceramic cores by stereolithography 3D printing. The effect of sintering temperature on the properties and microstructure of PSZ-reinforced ceramic cores was studied. The strengthening mechanism of PSZ on the cores was analyzed. The results will provide a reference for fabricating a high ceramic content core with a low solid content slurry by stereolithography 3D printing.

2 Experimental procedures

2.1 Sample fabrication

The fabrication process of sample includes slurry fabrication, curing, degreasing and sintering. The solid phase of the slurry was Al_2O_3 powder with purity of 99.55wt.%, and the liquid phase was photosensitive resin. In this study, the solid content of the ceramic slurry was 45vol.%. The photosensitive resin contained the crosslinker edoxylated (5) pentateradiol tetraacrylate (PPTTA) (DSM-AGI) and the precursor polysilazane (PSZ) (Anhui Ayotta Silicon Oil Co., Ltd.). The content of PSZ in the ceramic slurry was 10vol.%. The BASK dispersant (EFKA FA 4608, BASF, The Netherlands) was used. The Al_2O_3 powder after drying was mixed with photosensitive resin. The abrasive machine (Changsha Michi Instrument Equipment Co., Ltd.) was used for ball grinding. The rotation speed was 400 rpm and the ball grinding time was 12 h. The ZrO_2 balls with 8 mm in diameter were used as the grinding ball, and the mass ratio of the ZrO_2 balls to the slurry was 1:3. Finally, the prepared ceramic slurry was printed using a stereolithography 3D printer (Beijing TenDimensions Technology Co., Ltd.). Figure 1 shows the schematic diagram of the stereolithography 3D printer. A bottom-up mode for printing was used, and the shape of the curing layer was controlled by UV light [21]. Printing parameters were as follows: the thickness of a single-layer was 100 μm, the exposure time was 6 s, the power was 12 mW·cm^{-2}, and the depth of slurry in feeder bowl was 150 μm.

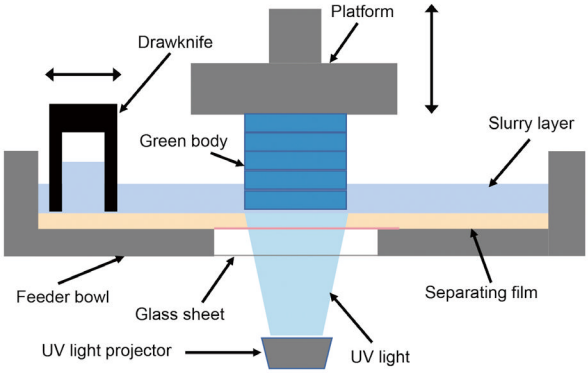

Fig. 1: Schematic diagram of stereolithography 3D printer

After the green bodies were prepared, they were degreased and sintered and then furnace cooling, as shown in Fig. 2. In the first stage, the green bodies were heated to 500 °C at 2 °C·min^{-1} and held for 750 min. In the second stage, the green bodies were heated to 1,000 °C at 1 °C·min^{-1} and held for 1,000 min. In the third stage, the green bodies were heated to the sintering temperature T (T=1,300 °C; 1,350 °C; 1,400 °C; 1,450 °C; 1,500 °C) at 0.5 °C·min^{-1} and held for 400 min. After sintering, the cores were cooled to 400 °C at 5 °C·min^{-1}, and then cooled with the furnace.

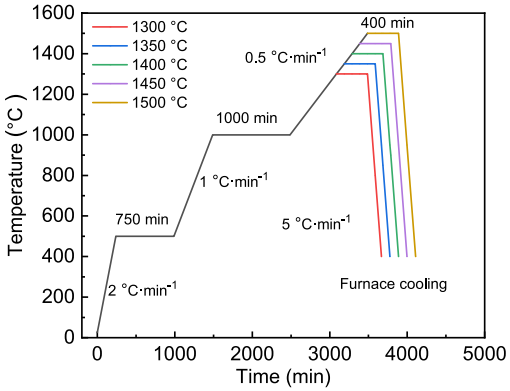

Fig. 2: Degreasing-sintering process of ceramic cores

2.2 Property test

Archimedes drainage method was used to measure the bulk density and open porosity of the ceramic cores [22]. The bulk density (ρ) and open porosity ($W\alpha$) of the ceramic core were calculated by Eqs. (1) and (2), respectively:

$$\rho = \frac{m_1}{m_3 - m_2} \times \rho_{water} \times 100\% \quad (1)$$

$$W\alpha = \frac{m_3 - m_1}{m_3 - m_2} \times 100\% \quad (2)$$

where, m_1 is the weight of the dried ceramic core, m_2 is the weight of the ceramic core in water, m_3 is the weight of the ceramic core filled with deionized water in the air, and ρ_{water} is the density of deionized water.

According to the weight of the ceramic core sample before and after sintering, the weight loss rate (W) of the ceramic core was calculated by Eq. (3):

$$W = \frac{n_1 - n_2}{n_1} \times 100\% \quad (3)$$

where, n_1 is the weight of green body, and n_2 is the weight of sintering ceramic core.

A vernier caliper was used to measure the size of the sample in the $X/Y/Z$ directions before and after sintering, and Eq. (4) was used to calculate the shrinkage rate (δ):

$$\delta = \frac{L - L_1}{L} \times 100\% \quad (4)$$

where L is the length of green body (mm), and L_1 is the length of ceramic core after sintering (mm).

Three points flexural method was used to test the flexural strength of the samples at 25 °C and 1,500 °C, respectively, as shown in Eq. (5):

$$\sigma_w = \frac{3PL}{2bh^2} \quad (5)$$

where, σ_w is the flexural strength (MPa), P is the load at fracture of ceramic core (N), b is the width of ceramic core (mm), and h is the thickness of ceramic core (mm). The experiment was performed at L=20 mm.

2.3 Characterization of microstructure and phase constitution

A field emission scanning electron microscope (FE-SEM; Quanta FEG 250, FEI Co., Ltd., USA) was used to analyze the fracture surface of the ceramic core after the flexural strength test. To study the effect of temperature on the properties of PSZ-reinforced ceramic cores, transmission electron microscopy (TEM; Themis Z, FEI, USA) and X-ray energy dispersive spectroscopy (EDS) were used to characterize the sintering state and the elemental distribution. The X-ray diffraction (XRD; SmartLab, Rigaku Instrument Corp., Japan) was used to determine the phase constitution of the ceramic core sample after sintering, under the scanning speed of 10°·min^{-1} and scanning angle of 10°–90°.

3 Results and discussion

3.1 Microstructure and phase constitution

The fracture morphology of ceramic cores at different sintering temperatures after flexural test was observed by SEM, as shown in Fig. 3. It can be found that there are some pores in the ceramic core after degreasing and sintering. The number of pores decreases with the increase of sintering temperature. The

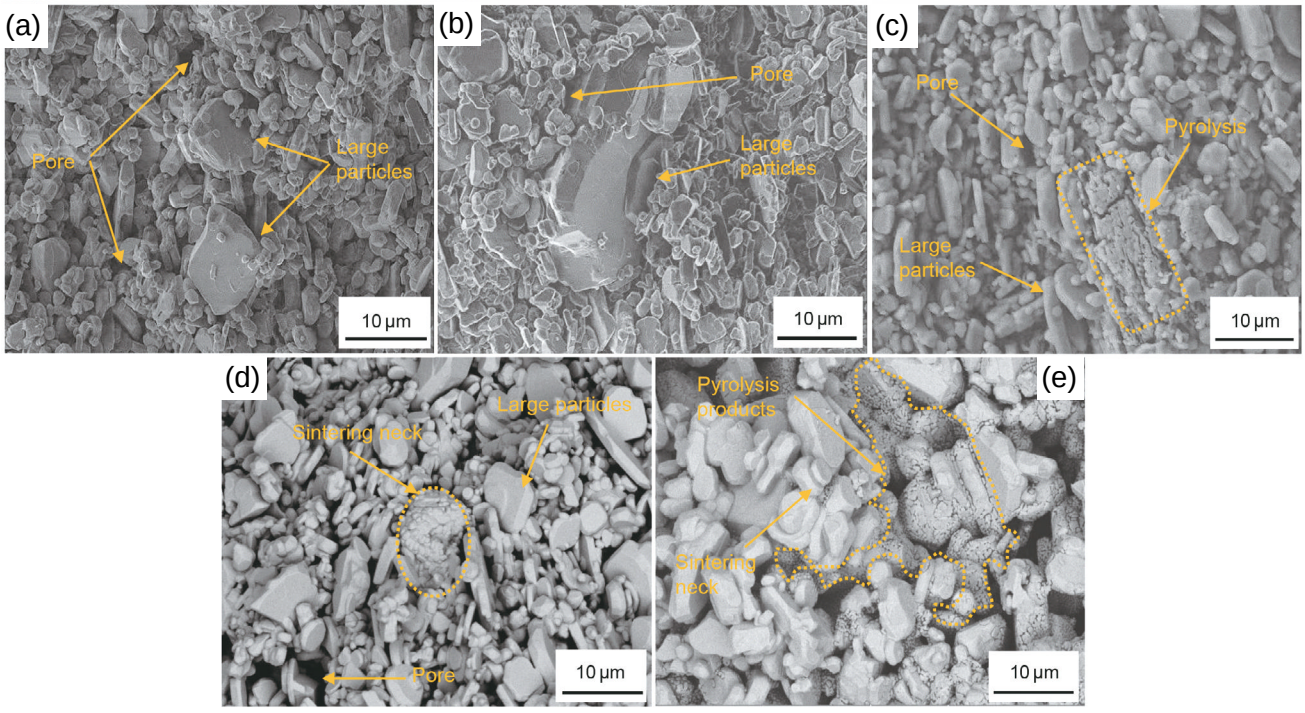

Fig. 3: Fracture morphologies of PSZ-reinforced ceramic cores after sintering at different temperatures: (a) 1,300 °C; (b) 1,350 °C; (c) 1,400 °C; (d) 1,450 °C; (e) 1,500 °C

formation of pores is related to two factors: On the one hand, during the process of degreasing, the cured photosensitive resin in ceramic cores is removed due to its instability at high temperatures (200–500 °C). Therefore, pores are formed in the position occupied by the cured photosensitive resin. On the other hand, irregular Al_2O_3 particles joined together can also lead to the formation of pores [23, 24]. In addition, the phenomenon of grain growth can be observed, which can be explained by the Arrhenius-type kinetic analysis model [25], as shown in Eq. (6):

$$G_t^m - G_0^m = Kt \quad (6)$$

where, G_t^m and G_0^m are the grain size at time t and 0, respectively, m is the grain growth index, and K is a constant. According to Eq. (6), the grain size increases with the increase of sintering temperature at a constant sintering rate and time. In the fracture surface of ceramic cores sintered at 1,300 °C and 1,350 °C [Figs. 3(a) and (b)], it can be seen that the surface of large ceramic particles is smooth and no other substances exist in the core. This may be because the pyrolysis behavior of the PSZ does not occur at this sintering temperature. As the sintering temperature exceeds 1,400 °C, the large particles are regarded as the skeleton in the microstructure of the core, and the small particles are attached to the surface or fill between the large particles [Figs. 3(c) and (d)]. This may be because PSZ has been pyrolyzed at high sintering temperatures. The sintering necks are formed among some large particles [Figs. 3(d) and (e)].

Figure 4 shows the morphology and elemental distribution of the ceramic cores sintered at 1,450 °C. As shown in Fig. 4(a), several microcracks are observed in bright particles, furthermore, the mergence of particles and sintering necks between large particles are observed. The strength of ceramic cores is directly determined by the strength of sintered necks [26]. EDS results show the bright particles are Al_2O_3 [Figs. 4(b) and (c)], the black area between the particles is the pore, and the gray sintering necks are the overlap of Si, N and C [Figs. 4(d, e and f)]. Thus, SiCN was generated by pyrolysis of PSZ at 1,450 °C. The Al-rich, Si-rich and O-rich areas are coincide, indicating that mullite phase may be generated.

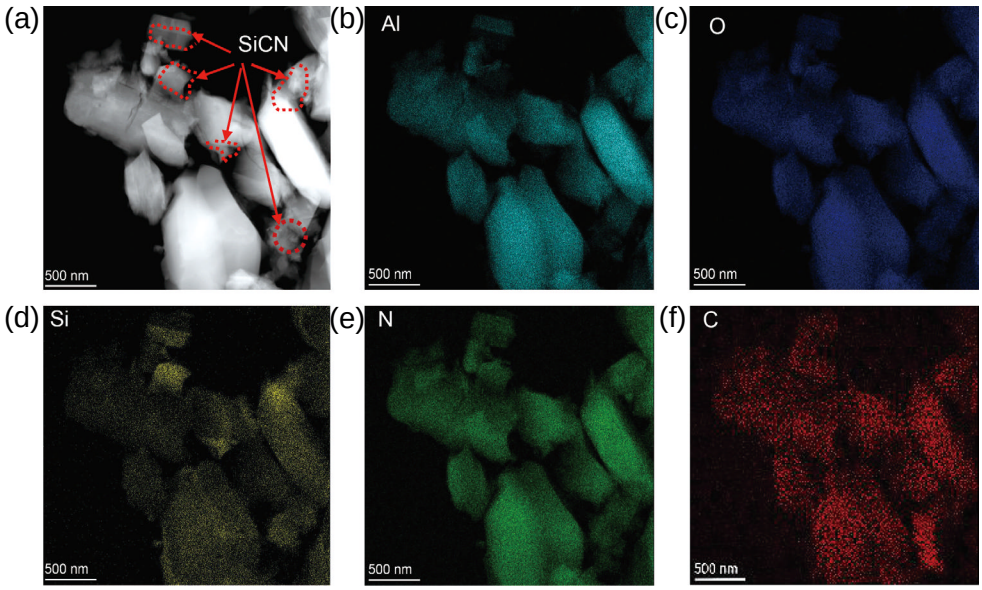

Fig. 4: Morphology and elemental distribution of ceramic cores sintered at 1,450 °C: (a) TEM image; (b) Al; (c) O; (d) Si; (e) N; (f) C

Figure 5 shows the XRD patterns of PSZ-reinforced ceramic cores at different sintering temperatures. When the sintering temperature is 1,300 °C and 1,350 °C, only Al_2O_3 can be detected. As the sintering temperature increases to 1,400 °C, a small amount of SiO_2 is detected because PSZ is pyrolyzed. When the sintering temperature increases to 1,450 °C, mullite is detected and the content of SiO_2 decreases. This is because the SiO_2 particles attached to the surface of Al_2O_3 particles react with Al_2O_3 to generate the mullite ($3Al_2O_3{\cdot}2SiO_2$). Thus, the content of SiO_2 decreases with the increase of sintering temperature. As the sintering temperature further increases to 1,500 °C, mullite and SiO_2 particles are also detected in the PSZ-reinforced ceramic core, but the content of SiO_2 decreases and mullite increases compared with that at 1,450 °C.

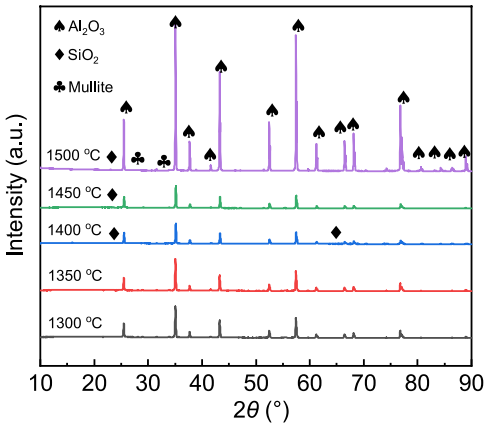

Fig. 5: Phase constitution of PSZ-reinforced ceramic cores after sintering

3.2 Comprehensive physical properties analysis

Figure 6 shows the bulk density and open porosity of PSZ-reinforced ceramic cores at different sintering temperatures. From 1,300 °C to 1,500 °C, the bulk density of PSZ-reinforced ceramic cores is monotonously increased from 2.13 g·cm^{-3} to 2.41 g·cm^{-3}, and the open porosity is decreased from 41.57% to 34.61%. The variation trend of open porosity is consistent with the classical sintering theory [9, 27]. It is also observed that the growth rate of the bulk density is a nonlinear function of sintering temperature. This is because higher sintering temperatures provide more energy during the heating process [28], and the densification of the PSZ-reinforced ceramic cores is driven by this energy [28]. The process of densification mainly includes particles growth, pores closure, and bulk shrinkage [29, 30]. Therefore, the increase of energy would cause the shrinkage of the ceramic and the increase of the bulk density of ceramics. Li et al. [31] have sintered green bodies of 3D-printed Al_2O_3-based ceramics at different temperatures and compared their bulk densities. Results showed that the bulk density of the ceramics was higher at higher sintering temperature, which are consistent with the conclusion of this work. Therefore, the sintering temperature is the key factor that determins the bulk density of sintered ceramics. Figure 6 also shows that the open porosity decreases with the increase of sintering temperature. Because higher sintering temperature promotes the growth of particles and reduce the distance between particles [28], resulting in the formation of sintering neck between adjacent particles. The sintering neck would occupy the place of the original hole, which reduce the open porosity. Hence, the bulk density and open porosity of ceramics are closely related to the sintering temperature, and their variation trend with sintering temperature is opposite. The open porosity changes from 41.57% to 34.61% with an increase in sintering temperature, which are all greater than 30%, can meet the application requirements [14].

The shrinkage rate in the *X*/*Y*/*Z* directions of PSZ-reinforced ceramic core after sintered at different temperatures is shown in Fig. 7(a). It can be found the shrinkage rate increases with the increase of sintering temperature at all of the *X*/*Y*/*Z* directions, which is consistent with the result that the higher the sintering temperature, the higher the bulk density of ceramic core. The higher sintering temperature provides a greater driving force or energy for sintering ceramic cores. Thus, the diffusion rate of atom between Al_2O_3 particles is accelerated, which is conducive to the densification process and the formation of sintering necks between adjacent particles [32]. The cross-sectional area of the sintering neck also increases with the increase of sintering temperature, which further promotes the densification process, and then increases the linear shrinkage [32]. The shrinkage rate is the maximum in the Z direction due to that the binding force between 3D-printed ceramic layers is weak [33, 34].

The weight loss rate of PSZ-reinforced ceramic cores after sintered at different temperatures is shown in Fig. 7(b). As the sintering temperature increases from 1,300 °C to 1,500 °C, the average weight loss rate of cores is 24.46%, 24.56%, 24.23%, 22.11%, 24.16%, respectively. The difference between the largest and the smallest value is 2.45%, indicating that the variation range in the weight loss rate of PSZ-reinforced ceramic cores is very small at different sintering temperatures. The weight loss is mainly caused by the decomposition of organic substances such as photosensitive resin and dispersant during degreasing.

Figure 8 shows the flexural strength of PSZ-reinforced ceramic cores sintered at different temperatures. When the sintering temperature increases from 1,300 °C to 1,450 °C, the flexural strength of PSZ-reinforced ceramic cores increases. The average flexural strength increases from 13.43 MPa to 32.70 MPa at 25 °C and from 2.05 MPa to 13.65 MPa at 1,500 °C. A too low sintering temperature results in insufficient sintering of core samples, and the binding force between Al_2O_3 particles in the PSZ-reinforced ceramic cores is weak. Thus, the flexural

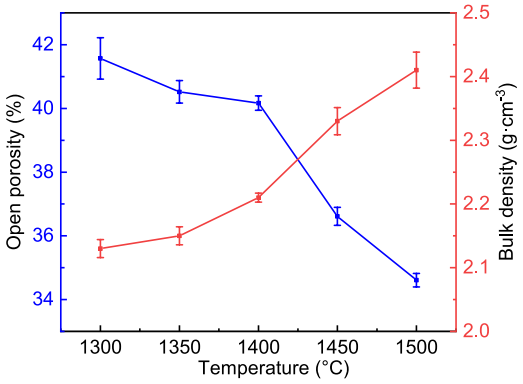

Fig. 6: Bulk density and open porosity of PSZ-reinforced ceramic cores after sintering at different temperatures

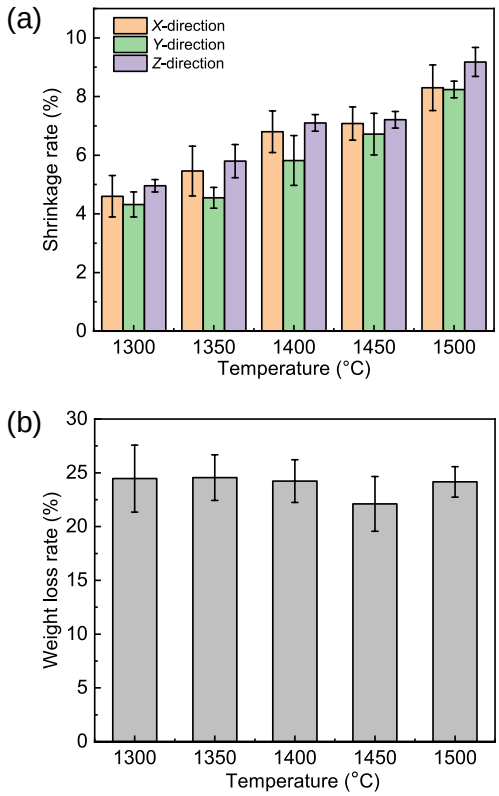

Fig. 7: Shrinkage rate (a) and weight loss rate (b) of PSZ-reinforced ceramic cores at different sintering temperatures

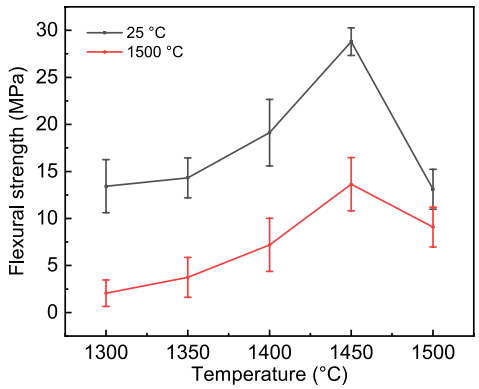

Fig. 8: Flexural strength of PSZ-reinforced ceramic cores at different sintering temperatures

strength of the cores is low. With the increase of sintering temperature, the atom diffusion coefficient between particles increases, the sintering process of the core samples is promoted, which enhances the binding force between particles [35]. As a result, the flexural strength of the cores is increased. When the sintering temperature reaches 1,400 °C, as shown in Fig. 3(c) and Fig. 5, a small amount of SiO_2 is detected due to the pyrolysis of PSZ. During the sintering process, SiO_2 particles fill the pores between Al_2O_3 particles and restrict the growth of particles in the ceramic core, therefore, improves the flexural strength of PSZ-reinforced ceramic cores. The flexural strength of the ceramic cores reaches the peak when the sintering temperature is 1,450 °C, which is 28.394 MPa at 25 °C and 13.649 MPa at 1,500 °C. As shown in Fig. 3(d), a large number of pyrolysis products are observed in the SEM images. They distribute among adjacent Al_2O_3 particles to form sintering necks, thus resulting in high flexural strength of ceramic core [32].

According to Figs. 4 and 5, the sintering necks are mainly composed of SiO_2, SiCN, SiCNO and mullite phase. Due to that the mullite has a higher strength at high-temperature [3], it plays an important role in improving the flexural strength. When the sintering temperature continues to increase, the average flexural strength of the ceramic cores is decreased at both 25 °C and 1,500 °C. This is because the amounts of SiCN and SiCNO produced by the pyrolysis of PSZ is increased when sintering at 1,500 °C, therefore, the content of SiO_2 and mullite are increased [36].

3.3 Sintering mechanism

Figure 9 schematically shows the sintering mechanism of PSZ-reinforced ceramic cores in different sintering stages. Firstly, the ceramic slurry is printed to green bodies by stereolithography 3D printing. Next, the green bodies are degreased and sintered in the sintering furnace. The aim of degreasing is to remove the cured photosensitive resin contained in the green bodies. In this process, the distance between Al_2O_3 particles becomes shorter, and the bulk of the green bodies becomes smaller. Then, the green bodies are sintered to densify the ceramic particles, as shown in Fig. 9(b). When the sintering temperature is below 1,400 °C, the microstructure and phase constitution of the core have no obvious change, as shown in Figs. 3(a, b) and 5. When the sintering temperature reaches 1,400 °C, a small amount of SiO_2 is detected by XRD, and PSZ starts to pyrolyze. In the initial stage of pyrolysis of the PSZ, N and C react with oxygen to generate NO_2 and CO_2, as shown in Eqs. (7) and (8) [37]:

$$N+O_2=NO_2 \quad (7)$$

$$C+O_2=CO_2 \quad (8)$$

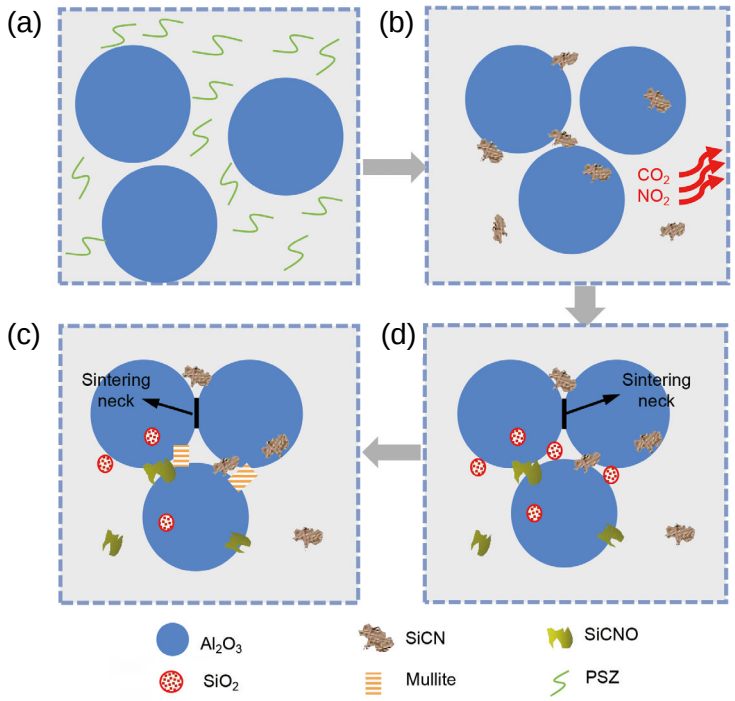

Fig. 9: Schematic diagram showing the sintering mechanism of PSZ-reinforced ceramic core in different sintering stages: (a) green body; (b) early stage of sintering; (c) middle stage of sintering; (d) final stage of sintering

After the volatilization of these two gases, some pores would be left in the ceramic cores. With the temperature increasing, the Si-N bond in PSZ breaks and reacts with the inserted C==O unit to generate SiCN [38], as shown in Eq. (9):

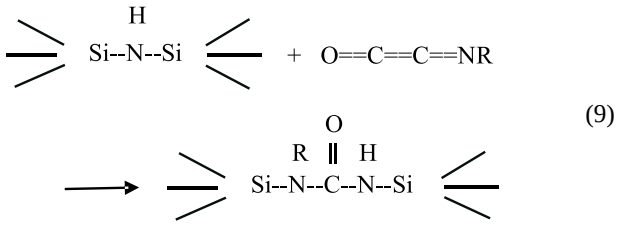

(9)

With further increase of sintering temperature, the area where SiCN is in contact with the pores is oxidized to generate SiCNO [Eq. (10)], and the remaining Si reacts with oxygen to generate SiO_2 [Eq. (11)] [39]:

$$2SiCN+O_2=2SiCNO \quad (10)$$

$$Si+O_2=SiO_2 \quad (11)$$

The SiO_2 particles are diffusely distributed in the cores, as shown in Fig. 9(c). The SiO_2 particles attach to the surface of Al_2O_3 particles and then react with Al_2O_3 to generate mullite ($3Al_2O_3{\cdot}2SiO_2$), as shown in Eq. (12) [40, 41]:

$$3Al_2O_3+2SiO_2=3Al_2O_3{\cdot}2SiO_2 \quad (12)$$

The principle of the reaction is that the wetting force and the surface tension of the fused silica on the Al_2O_3 surface enable the Al_2O_3 granules to be close to each other, accelerating the dissolution of the Al^{3+} ions toward the SiO_2, and promoting the formation of the mullite [42-44]. During the sintering process, the distance between adjacent Al_2O_3 particles decreases [45], and the above-mentioned products (SiO_2, SiCN, SiCNO and mullite) are distributed on the surface of Al_2O_3 particles, further shortening the distance between adjacent Al_2O_3 particles, and thus forming the sintered necks with certain strength. The sintering necks are grown under the action of atomic diffusion. The products (SiO_2, SiCN, SiCNO and mullite) around the Al_2O_3 particles contribute to the formation of reticulated sintering necks, increasing the bonding area between the Al_2O_3 particles, which enhances the strength of PSZ-reinforced ceramic cores [15], as shown in Fig. 9(d).

4 Conclusions

A new idea of preparing cores with high ceramic content using the slurry with a low solid content was provided. Stereolithography 3D printing was used to fabricate PSZ-reinforced ceramic cores. The influence of sintering temperature on the properties and microstructure of PSZ-reinforced ceramic cores was studied, and the sintering mechanism was further explored. Following conclusions can be achieved:

(1) In PSZ-reinforced ceramic core, the sintering products (SiCN, SiCNO, SiO_2 and mullite) are distributed between Al_2O_3 particles, the sintering necks composed of these sintering products increases the bonding area between adjacent Al_2O_3 particles, thereby enhancing the strength of the cores.

(2) PSZ can be pyrolyzed as the sintering temperature reaches 1,400 °C. The pyrolysis products of PSZ include SiCN, SiCNO and SiO_2. The SiO_2 particles attach to the surface of Al_2O_3 particles and then react with the Al_2O_3 to generate mullite.

(3) The optimal sintering temperature of PSZ-reinforced ceramic core is 1,450 °C. At this sintering temperature, the open porosity of the ceramic core is 36.60%, flexural strength is 28.794 MPa at 25 °C and 13.649 MPa at 1,500 °C, which can meet the casting requirements of hollow blades.

Acknowledgements

This work was financially supported by the National Natural Science Foundation of China (No. U22A20129), National Science and Technology Major Project (No. 2017-VI-0002-0072), National Key Research and Development Program of China (No. 2018YFB1106600), Fundamental Research Funds for the Central Universities (WK5290000003), and Students' Innovation and Entrepreneurship Foundation of USTC (Nos. CY2022G10 and CY2022C24).

Conflict of interest

The authors declare that they have no known competing financial interests or personal relationships that could have appeared to influence the work reported in this paper.

References

[1] Zhang H, Xu Q Y, Liu B C. Numerical simulation and optimization of directional solidification process of single crystal superalloy casting. Materials, 2014, 7(3): 1625–1639.
[2] Zhao S, Siqueira G, Drdova S, et al. Additive manufacturing of silica aerogels. Nature, 2020, 584: 387–392.
[3] Li Q L, Meng X T, Zhang X C, et al. Enhanced 3D printed Al_2O_3 core via in-situ mullite. Additive Manufacturing, 2022, 55: 102826.
[4] Liu X F, Guo X L, Shui G Y, et al. Properties of alumina-based ceramic cores. China Foundry, 2021(6), 18: 593–598.
[5] Gromada M, Swieca A, Kostecki M, et al. Ceramic cores for turbine blades via injection moulding. Journal of Materials Processing Technology, 2015, 220: 107–112.
[6] Pan Z P, Guo J Z, Li S M, et al. Effect of nonuniform sintering on mechanical and thermal properties of silica-based ceramic cores. China Foundry, 2021, 18(5): 457–462.
[7] Gromada M, Świeca A, Kostecki M, et al. Ceramic cores for turbine blades via injection moulding. Journal of Materials Processing Technology, 2015, 220: 107–112.
[8] Meyer T V M, Dedecke D, Paul U, et al. Undercooling related casting defects in single crystal turbine blades. Superalloys, 1996: 471–479.
[9] Li Q L, An X L, Liang J J, et al. Balancing flexural strength and porosity in DLP-3D printing Al_2O_3 cores for hollow turbine blades. Journal of Materials Science & Technology, 2022, 104: 19–32.
[10] Xu Q Y, Zhang H, Liu B C. Multiscale modelling and simulation of single crystal superalloy turbine blade casting during directional solidification process. China Foundry, 2014, 11(4): 269–276.

[11] Wu B, Liang J J, Yang Y H, et al. Phase constitution, microstructure and mechanical properties of a Ni-based superalloy specially designed for additive manufacturing. China Foundry, 2021, 18(4): 397–408.
[12] Yu J, Xu Q Y, Liu B C, et al. Experimental study and numerical simulation of directionally solidified turbine blade casting. Journal of Materials Science & Technology, 2008, 24(3): 369–373.
[13] Li F, Huang X, Liu X, et al. Sol-gel derived porous ultra-high temperature ceramics. Journal of Advanced Ceramics, 2020, 9: 1–16.
[14] Li Q L, Liang J J, Zhang Y L, et al. Fused silica ceramic core based on network-structured zircon design via 3D printing. Scripta Materialia, 2022, 208: 114342.
[15] He C, Liu X E, Ma C, et al. Digital light processing of Si-based composite ceramics and bulk silica ceramics from a high solid loading polysiloxane/SiO_2 slurry. Journal of the European Ceramic Society, 2021, 41: 7189–7198.
[16] Hu L H, Wang Y K, Wang S C. Polymer derived gel-like preceramic precursor of core-shell silicon oxycarbide ceramic for robocasting. Ceramics International, 2019, 45: 23475–23481.
[17] He C, Liu X E, Ma C, et al. Digital light processing fabrication of mullite component derived from preceramic precusor using photosensitive hydroxysiloxane as the matrix and alumina nanoparticles as the filler. Journal of the European Ceramic Society, 2021, 41: 5570–5577.
[18] He C, Liu X E, Ma C, et al. Digital light processing of complex-shaped 3D-zircon ($ZrSiO_4$) ceramic components from a photocurable polysiloxane/ZrO_2 slurry. Ceramics International, 2021, 47: 32905–32914.
[19] Zambottia A, Biesuza M, Campostrini R, et al. Synthesis and thermal evolution of polysilazane-derived SiCN(O) aerogels with variable C content stable at 1600 °C. Ceramics International, 2021, 47(6): 8035–8043.
[20] Kousaalya A B, Kumar R, Sridhar B T N. Thermal conductivity of precursor derived Si-B-C-N ceramic foams using Metroxylon sagu as sacrificial template. Ceramics International, 2015, 41: 1163.
[21] Eckel Z, Zhou C, Martin J, et al. Additive manufacturing of polymer derived ceramics. Science, 2016, 351(6268): 58–62.
[22] Li X, Hu K, Lu Z. Effect of light attenuation on polymerization of ceramic suspensions for 3D printing. Journal of the European Ceramic Society, 2019, 39: 2503–2509.
[23] Li H, Liu Y S, Liu Y S, et al. Silica strengthened alumina ceramic cores prepared by 3D printing. Journal of the European Ceramic Society, 2021, 41: 2938–2947.
[24] Chen I, Wang X. Sintering dense nanocrystalline ceramics without final-stage grain growth. Nature, 2000, 404(6774): 168–171.
[25] Santanach J G, Weibel A, Estournes C, et al. Spark plasma sintering of alumina: study of parameters, formal sintering analysis and hypotheses on the mechanism(s) involved in densification and grain growth. Acta Materialia, 2011,59: 1400–1408.
[26] Ryshkewitch E. Compression strength of porous sintered alumina and zirconia. Journal of the American Ceramic Society, 1953, 36: 65–68.
[27] Ma J, Lim L C. Effect of particle size distribution on sintering of agglomerate-free submicron alumina powder compacts. Journal of the European Ceramic Society, 2002, 22: 2197–2208.
[28] Li H, Liu Y S, Li W B, et al. The effect of sintering on the properties of calcium oxide promoted alumina-based ceramic cores via 3D printing. Materials Chemistry and Physics, 2021, 263: 124443.
[29] Guo S. Densification of ZrB_2-based composites and their mechanical and physical properties: A review. Journal of the European Ceramic Society, 2009, 29(6): 995–1011.
[30] Funahashi S, Guo J, Guo H, et al. Demonstration of the cold sintering process study for the densification and grain growth of ZnO ceramics. Journal of the American Ceramic Society, 2017, 100(2): 546–553.
[31] Li H, Liu Y, Liu Y, et al. Effect of sintering temperature in argon atmosphere on microstructure and properties of 3D printed alumina ceramic cores. Journal of Advanced Ceramics, 2020, 9(2): 220–231.
[32] Yang Z G, Zhao Z J, Yu J B, et al. Effect of silicone resin as precursor and binder on the properties of alumina-based ceramic cores using ball-shaped powders. Ceramics International, 2019, 45: 2170–2177.
[33] Li Q L, Chen T C, Liang J J, et al. Manufacturing of ceramic cores: From hot injection to 3D printing. Journal of Materials Science & Technology, doi: 10.1016/ j.jmst. 2022.06.033.
[34] Li Q L, Hou W Q, Liang J J, et al. Controlling the anisotropy behaviour of 3D printed ceramic cores: From intralayer particle distribution to interlayer pore evolution. Additive Manufacturing, doi: 10.1016/ j.addma. 2022.103055.
[35] Fu Y, Xu G, Chen Z, et al. Multiple metals doped polymer-derived SiOC ceramics for 3D printing. Ceramics International, 2018, 44: 11030–11038.
[36] Huang M Z, Wu Y Y, Ou J, et al. 3D-printing of polymer-derived SiCN ceramic matrix composites by digital light processing. Journal of the European Ceramic Society, 2022, 42: 5476–5483.
[37] Li Q L, Pan Z X, Liang J J, et al. Ceramic composites toughened by vat photopolymerization 3D printing technology. Journal of Materials Science & Technology, 2023, 146: 42–48.
[38] Klebe J F, Bush J B, Lyons J E. The addition of silylamines and silazanes to isocyanates. Journal of American Chemical Society, 1964, 86: 4400–4406.
[39] Herrmann M, Schönfeld K, Klemm H, et al. Laser-supported joining of SiC-fiber/SiCN ceramic matrix composites fabricated by precursor infiltration. Journal of the European Ceramic Society, 2014, 34: 2913–2924.
[40] Liu J Q, Li Q L, Huo M D, et al. Microstructure and mechanical properties of 3D-printed nano-silica reinforced alumina cores. Ceramics International, doi: 10.1016/ j.ceramint. 2022.06.301.
[41] Li Q L, Gu Y, Yu X H, et, al. Effect of sintering temperature on surface morphology and roughness of 3D-printed silicon ceramic cores. Journal of Inorganic Materials, 2022, 37(3): 325–332.
[42] Hotta Y, Banno T, Oda K. Physical properties of slip casting of high pure Al_2O_3 slurry using porous Al_2O_3-glass mold. Journal of Materials Science, 2002, 37: 417–423.
[43] Qin Y X, Pan W. Effect of silica sol on the properties of alumina-based ceramic core composites. Materials Science and Engineering A, 2009, 508(1): 71–75.
[44] Low I M, Lim F W, Low S S. Synthesis of highly leachable gel-derived alumina ceramic cores. Journal of Materials Science Letters, 1993, 12(20): 1570–1573.
[45] Zhang K, Xie C, Wang G, et al. High solid loading, low viscosity photosensitive Al_2O_3 slurry for 3D printing based additive manufacturing. Ceramics International, 2019, 45: 054051203–054051208.